Neuron
Article

Metaplasticity at Single Glutamatergic Synapses

Ming-Chia Lee,[1] Ryohei Yasuda,[1,2] and Michael D. Ehlers[1,2,*]
[1]Department of Neurobiology
[2]Howard Hughes Medical Institute
Duke University Medical Center, Durham, NC 27710, USA
*Correspondence: ehlers@neuro.duke.edu
DOI 10.1016/j.neuron.2010.05.015

SUMMARY

Optimal function of neuronal networks requires interplay between rapid forms of Hebbian plasticity and homeostatic mechanisms that adjust the threshold for plasticity, termed metaplasticity. Numerous forms of rapid synapse plasticity have been examined in detail. However, the rules that govern synaptic metaplasticity are much less clear. Here, we demonstrate a local subunit-specific switch in NMDA receptors that alternately primes or prevents potentiation at single synapses. Prolonged suppression of neurotransmitter release enhances NMDA receptor currents, increases the number of functional NMDA receptors containing NR2B, and augments calcium transients at single dendritic spines. This local switch in NMDA receptors requires spontaneous glutamate release but is independent of action potentials. Moreover, single inactivated synapses exhibit a lower induction threshold for both long-term synaptic potentiation and plasticity-induced spine growth. Thus, spontaneous glutamate release adjusts plasticity threshold at single synapses by local regulation of NMDA receptors, providing a novel spatially delimited form of synaptic metaplasticity.

INTRODUCTION

Synaptic plasticity is a cellular substrate for learning and memory. While Hebbian plasticity is recognized as a cellular mechanism for storing information at individual synapses (Kessels and Malinow, 2009; Malenka and Bear, 2004), metaplastic mechanisms that adjust the threshold of synaptic plasticity have been proposed to increase information storage capacity and enable acquisition of stimulus-selective responses (Abraham, 2008; Fusi and Abbott, 2007; Fusi et al., 2005; Montgomery and Madison, 2002). Several forms of Hebbian synapse plasticity and their underlying molecular mechanisms have been described in exquisite detail (Kessels and Malinow, 2009; Malenka and Bear, 2004; Newpher and Ehlers, 2008; Shepherd and Huganir, 2007). However, the synaptic rules and molecular mechanisms that govern metaplasticity are much less clear. Indeed, whether and how metaplasticity occurs at the level of single synapses remains elusive, although theoretical models suggest that the existence of such mechanisms is essential for optimal memory performance (Fusi et al., 2005).

At excitatory synapses in the mammalian brain, two major ionotropic glutamate receptors—AMPA-type receptors (AMPARs) and NMDA-type receptors (NMDARs)—play critical roles in synaptic plasticity. At many glutamatergic synapses, Hebbian forms of plasticity such as long-term potentiation (LTP) and long-term depression (LTD) are expressed by synapse-specific regulation of the number of synaptic AMPARs (Kessels and Malinow, 2009; Malenka and Bear, 2004; Matsuzaki et al., 2004; Newpher and Ehlers, 2008; Shepherd and Huganir, 2007). Whereas AMPARs mediate the bulk of the charge transfer during rapid excitatory synaptic transmission and thus determine synaptic strength, NMDARs mediate a slower component of excitatory transmission and trigger intracellular signaling pathways by virtue of their high Ca^{2+} permeability. Indeed, activation of NMDARs is required for the induction of diverse forms of synapse plasticity including LTP and LTD (Abraham, 2008; Malenka and Bear, 2004; Yashiro and Philpot, 2008). It is well established that signaling via NMDARs changes during brain development, and these changes are crucial for experience-dependent circuit plasticity (Monyer et al., 1994; Sheng et al., 1994; Yashiro and Philpot, 2008). NMDAR channel properties and associated Ca^{2+} influx are influenced by diverse intracellular signaling pathways (Ehlers et al., 1996; Salter and Kalia, 2004; Skeberdis et al., 2006), and fine-tuning of NMDAR function regulates the threshold for inducing synaptic plasticity (Abraham, 2008; Yashiro and Philpot, 2008). Despite being an attractive substrate for synaptic metaplasticity, it remains unclear whether and how prior activity regulates NMDARs at single synapses.

One major mechanism for regulating NMDAR function is altering subunit composition. NMDARs are tetramers typically composed of two obligatory NR1 subunits and two NR2 subunits (NR2A-D) (Cull-Candy and Leszkiewicz, 2004; Liu et al., 2004a; Morishita et al., 2007). NR2 subunits are key determinants of NMDAR channel properties and signaling. For example, NR1/NR2A diheteromers have higher peak open probability upon activation and possess shorter rise and decay times than receptors containing NR2B (Erreger et al., 2005). Conversely, NR1/NR2B diheteromers have slower decay kinetics (Erreger et al., 2005; Prybylowski et al., 2002; Sobczyk et al., 2005) and exhibit a strong interaction with Ca^{2+}/calmodulin-dependent protein kinase type II (CaMKII) (Barria and Malinow, 2005; Bayer et al., 2001). Given the importance of NMDAR-dependent Ca^{2+} influx and CaMKII activation in LTP (Lisman et al., 2002; Malenka and Bear, 2004; Shepherd and Huganir, 2007), these properties have led to the suggestion that activation of NMDARs containing

NR2B favors LTP induction (Barria and Malinow, 2005; Foster et al., 2010; Yashiro and Philpot, 2008; Zhou et al., 2007). On the other hand, NR2A-containing NMDARs have also been found to contribute to LTP induction (Erreger et al., 2005; Kim et al., 2005; Liu et al., 2004a); the precise contribution of different populations of NMDARs to synaptic plasticity thus remains unclear.

The subunit composition and accumulation of NMDARs at synapses is regulated by neuronal activity (Barria and Malinow, 2002; Bellone and Nicoll, 2007; Jung et al., 2008; Lau and Zukin, 2007; Mu et al., 2003; Rao and Craig, 1997; Watt et al., 2000; Yashiro and Philpot, 2008), and changes in NMDAR subunit composition have been shown to modify synaptic plasticity (Barria and Malinow, 2005; Gardoni et al., 2009; Jung et al., 2008; Liu et al., 2004a; Tang et al., 1999). To date, changes in NMDAR subunit composition and expression have been examined upon prolonged manipulations of global activity (Barria and Malinow, 2002; Colonnese et al., 2003; Groc et al., 2006; Hoffmann et al., 2000; Yashiro et al., 2005) or acutely following simultaneous activation of many synapses in a complex network (Bellone and Nicoll, 2007). It remains unknown whether and how NMDAR composition is tuned by ongoing activity at the level of single synapses, and if so, what effects this has on synaptic plasticity.

In the present study, we manipulated local synaptic activity and probed corresponding changes in NMDAR composition and plasticity threshold at single synapses. Using quantitative immunocytochemistry and local two-photon glutamate uncaging, we show that prolonged suppression of neurotransmitter release enhances NMDAR currents and increases the number of functional NMDARs containing NR2B on single dendritic spines. This local switch in NMDAR composition is independent of action potentials but requires spontaneous glutamate release. Furthermore, single inactivated synapses exhibit elevated calcium transients, have a lower induction threshold for long-term synaptic potentiation, and more readily undergo dendritic spine growth elicited by local glutamate uncaging. Thus, by modifying NMDAR composition, spontaneous glutamate release sets plasticity threshold on a synapse-by-synapse basis.

RESULTS

NMDAR Currents Are Enhanced at Single Silenced Synapses

To determine if input-specific activity modifies synaptic NMDAR composition, we simultaneously labeled and inactivated sparse populations of presynaptic boutons onto individual postsynaptic cells. For this, we transfected presynaptic cells with a construct that allows dual expression of a presynaptic marker (synaptophysin-GFP, SphGFP) and the tetanus toxin light chain (TeNT) (Ehlers et al., 2007). Dual expression was achieved by placing the TeNT cDNA downstream of an internal ribosome entry site (IRES) following synaptophysin-GFP. TeNT suppresses presynaptic release by selective proteolysis of the synaptic vesicle SNARE protein VAMP2 (Ehlers et al., 2007; Harms et al., 2005; Schoch et al., 2001). The efficacy of TeNT blockade of presynaptic vesicle release was confirmed with FM loading assays (see Figure S1A available online), consistent with our previous findings (Ehlers et al., 2007). Using sparse lentiviral infection in primary cultures, expression of SphGFP-IRES-TeNT was limited to a subpopulation of hippocampal neurons, which led to a small fraction of silenced boutons contacting any given postsynaptic neuron labeled by subsequent transfection with mCherry (Figure 1A). For individual mCherry-filled postsynaptic neurons, the contacting SphGFP-labeled presynaptic boutons thus represent silenced synapses due to the coexpression of TeNT, while neighboring synapses receiving inputs from uninfected neurons are spontaneously active (Figure 1A).

To probe glutamate receptor composition at silenced synapses, we performed whole-cell voltage clamp recordings and recorded currents evoked by focal two-photon glutamate uncaging on individual dendritic spines (see Experimental Procedures for details). Uncaging-induced postsynaptic currents (uEPSCs) reliably mimicked miniature excitatory postsynaptic currents (mEPSCs) in the same recordings (Figure S1B). To determine if local activity modifies glutamate receptor composition, we measured uEPSCs at neighboring active and silenced synapses. In each experiment, two nearby synapses (distance $< 5\ \mu m$), one silenced and one active, on dendritic spines with similar volume were chosen as a pair of interest (Figure 1B, left panel). In all cases, spine volume was measured using the fluorescence intensity of the mCherry cell fill at both active and silenced synapses and found to be no different (paired t test, $p > 0.1$). For each pair, uEPSCs were recorded at -70 mV ($uEPSC_{-70mV}$) to measure the contribution of AMPARs, and then at +40 mV ($uEPSC_{+40mV}$) to measure mixed uEPSCs consisting of both AMPAR- and NMDAR-mediated synaptic currents (Figure 1B). Although active and silenced synapses showed similar peak AMPAR-mediated responses recorded at -70 mV (AMPAR-uEPSCs, active, 10.9 ± 2.8 pA; silenced, 11.0 ± 2.3 pA, $p > 0.1$), currents recorded at +40 mV were larger at silenced synapses (Figures 1B and 1C). To determine the contribution of NMDARs, current amplitudes were measured 45 ms after the $uEPSC_{-70mV}$ peak, a time when AMPAR currents have decayed (Béïque et al., 2006; Poncer and Malinow, 2001). This analysis indicated that NMDAR-mediated currents were significantly enhanced at silenced synapses relative to adjacent active synapses (Figure 1C; NMDAR-uEPSCs: active, 8.5 ± 1.3 pA; silenced, 14.0 ± 1.9 pA; paired-t test, $p < 0.01$; n = 19 pairs from 16 neurons). Across the pairs recorded, silenced synapses consistently showed a higher NMDAR-uEPSC to AMPAR-uEPSC (NMDAR/AMPAR) ratio compared to the corresponding neighboring active synapse (Figure 1D). Together, these data show that synaptic activity selectively and locally suppresses NMDAR responses.

NMDARs Containing NR2B Subunits Accumulate at Inactive Synapses

Consistent with the observed increase in NMDAR-uEPSCs (Figure 1), silenced synapses showed stronger staining for the obligatory NMDAR subunit NR1 compared to adjacent active synapses (Figure 2A). Notably, higher levels of NR2B but not NR2A were observed at silenced synapses (Figure 2A), and this increase in NR2B was due to accumulation of surface receptors (Figure S2A). Changes in NMDAR subunit composition were quantified by normalizing receptor content at silenced synapses to the mean receptor content of active synapses on the same

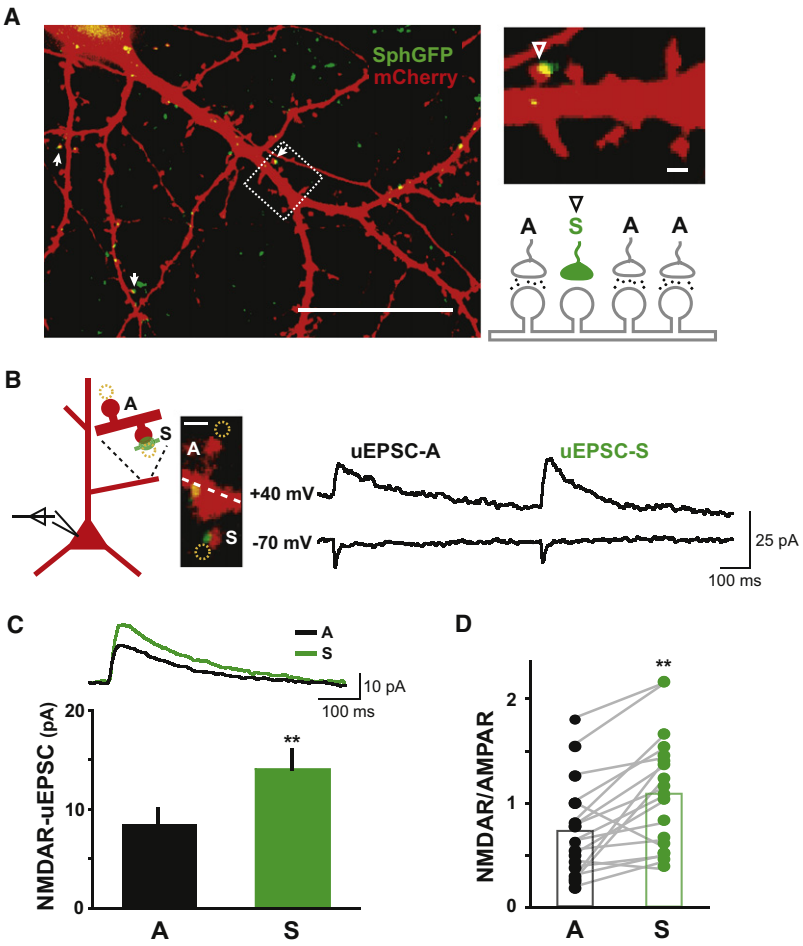

Figure 1. Local Inactivation Enhances NMDAR Currents at Single Synapses

(A) Illustration of the experimental system. Hippocampal neurons were sparsely infected with a lentivirus expressing synaptophysin-GFP-IRES-tetanus toxin light chain (SphGFP-IRES-TeNT) at DIV11-12. Individual postsynaptic neurons were visualized by subsequent mCherry transfection at DIV17–19. Left panel, 7–10 days after infection, a small fraction of the spines on mCherry-filled neurons contacted presynaptic boutons that were visible as green due to the expression of synaptophysin-GFP and silenced due to the co-expression of tetanus toxin light chain (TeNT) (arrows). The large majority of synapses originated from uninfected neurons, which were spontaneously active. Upper right, a magnified view from the boxed region showing a silenced synapse on a dendritic spine with a contacting green bouton (arrowhead) and neighboring active synapses. Lower right, schematic diagram of single-synapse inactivation. S, silenced; A, active. Scale bars: 50 μm left, 1 μm right.

(B) Paired recordings of synaptic currents at neighboring active and silenced synapses. Uncaging-evoked excitatory postsynaptic currents (uEPSCs) were recorded upon focal two-photon glutamate uncaging at nearby active (A) and silenced (S) synapses on dendritic spines. For each pair, average uEPSCs were sequentially recorded from active (uEPSC-A) and silenced synapses (uEPSC-S) at holding potentials of −70 mV (bottom trace) and +40 mV (top trace). Scale bar, 1 μm.

(C) Enhanced NMDAR-mediated uEPSCs at silenced synapses. Upper panel, average uEPSCs of active (A, black) and silenced (S, green) synapses from 19 A-S pairs recorded at +40 mV. Bottom panel, means ± SEM of the NMDAR-mediated component of the uEPSC measured 45 ms after the peak. Active (A), 8.5 ± 1.3 pA; silenced (S), 14.0 ± 1.9 pA; **$p < 0.01$, paired t test; n = 19 A-S pairs from 16 neurons.

(D) Across pairs of active (A) and silenced (S) synapses recorded, silenced synapses consistently showed higher NMDAR/AMPAR uEPSC ratios than neighboring active synapses. A, 0.7 ± 0.1; S, 1.1 ± 0.1; paired t test, **$p < 0.01$.

neuron (normalized synaptic content, $S/\overline{A}$) for NR1, NR2A, and NR2B. As shown in the cumulative plot of $S/\overline{A}$ (Figure 2B1), the distribution of NR1 and NR2B intensity was shifted to the right with median $S/\overline{A} > 1$, indicating that silenced synapses contain more NR1 (n = 475 synapses on 39 neurons) and NR2B (n = 343 synapses on 35 neurons) compared to active synapses. The distribution of NR1 intensity overlapped with the NR2B distribution ($p > 0.05$, Kolmogorov-Smirnov test) but deviated from the NR2A trace ($p < 0.05$ compared to both NR1 and NR2B, Kolmogorov-Smirnov test). The distribution of $S/\overline{A}$ values for NR2A peaked around 1.0 (Figure 2B2; $S/\overline{A}_{NR2A} \leq 1$ for 45% of synapses), indicating similar NR2A levels at active and silenced synapses. In contrast, the NR1 and the NR2B distributions both peaked near 2.0 (Figures 2B3 and 2B4; $S/\overline{A}_{NR1} \geq 1$ for 82% of synapses; $S/\overline{A}_{NR2B} \geq 1$ for 83% of synapses), indicating that silenced synapses accumulated approximately 2-fold more NR1 and NR2B compared to average active synapses. This selective accumulation of NR1 and NR2B at silenced synapses was consistently observed on a per neuron basis (Figure 2C; $S/\overline{A}_{NR1}$, 1.90 ± 0.08, n = 39; $S/\overline{A}_{NR2A}$, 1.16 ± 0.04, n = 34; $S/\overline{A}_{NR2B}$, 1.88 ± 0.08, n = 35; $p_{NR1\text{-}NR2A} < 0.01$, $p_{NR2A\text{-}NR2B} < 0.01$, $p_{NR1\text{-}NR2B} > 0.1$). The accumulation of NR1 and NR2B was spatially confined to silenced synapses and did not occur at adjacent active synapses (Figures 2D and 2E). Moreover, RNAi-mediated knock down of NR2B prevented the inactivity-induced accumulation of NR1 (Figure S2B), indicating a strict requirement for the NR2B subunit. Together, these findings demonstrate that prolonged inactivity increases the number of NR2B-containing NMDARs at single synapses.

Spontaneous Glutamate Release Triggers a Local Switch in NMDARs

Presynaptic expression of TeNT affects both action potential-evoked and spontaneous glutamate release (Capogna et al., 1997; Ehlers et al., 2007; Harms and Craig, 2005; Schoch et al., 2001). Thus, the relative reduction in NR2B-containing NMDARs at active synapses could arise from spike-evoked release, spontaneous release, or a combination of the two. To distinguish these possibilities, we alternately inhibited network activity by applying tetrodotoxin (TTX) or blocked postsynaptic

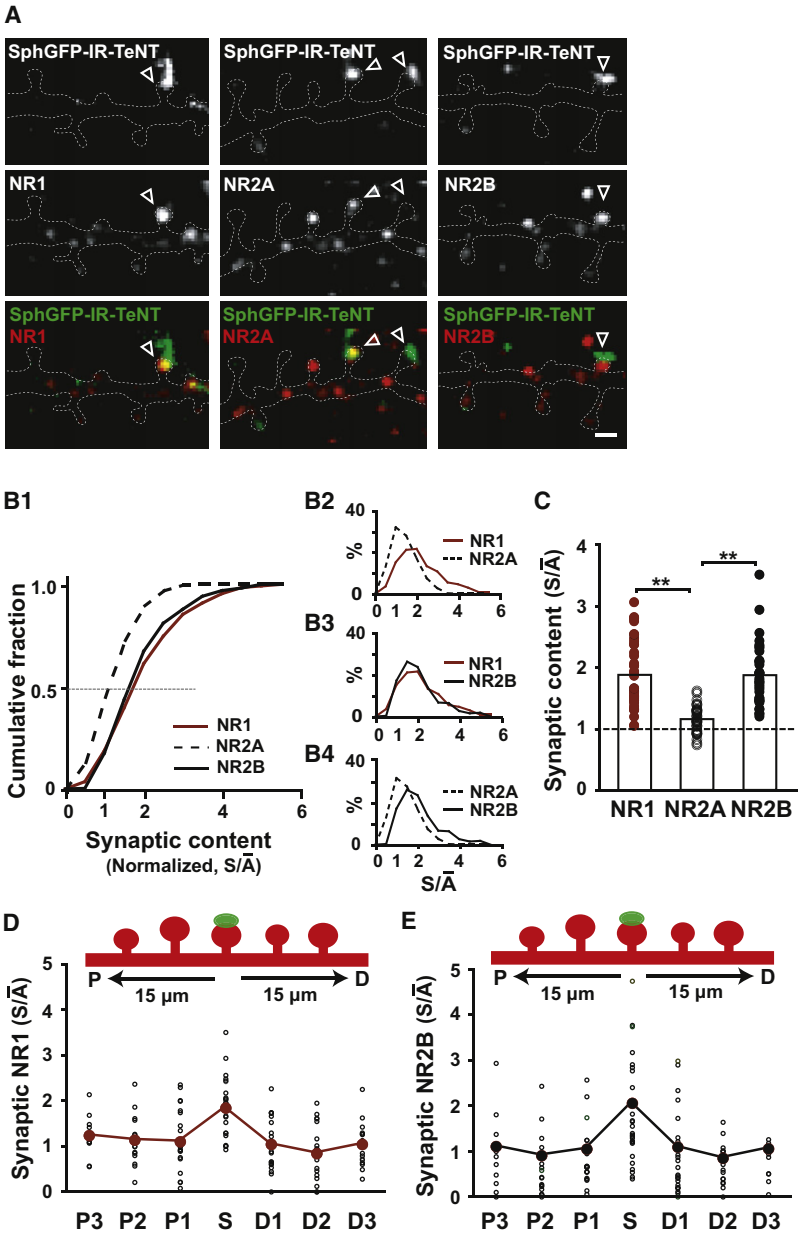

Figure 2. Single Silenced Synapses Accumulate NR1 and NR2B but Not NR2A

(A) Immunocytochemistry for NR1, NR2A, and NR2B at silenced and active synapses. Silenced synapses (arrowheads) contain more NR1 and NR2B compared to neighboring active synapses on dendritic spines. The dashed white line indicates the dendritic outline. Scale bar, 1 µm.

(B) Subunit-specific accumulation of NMDARs at silenced synapses. The synaptic content of NR1, NR2A, and NR2B detected by immunocytochemistry was quantified at silenced synapses and normalized to mean values at active synapses (S/$\bar{A}$; see Experimental Procedures for details). The cumulative plot (B1) shows overlapping right-shifted NR1 and NR2B distributions ($p > 0.05$, Kolmogorov-Smirnov test), which significantly deviate from the NR2A trace ($p < 0.05$ relative to both NR1 and NR2B, Kolmogorov-Smirnov test). (B2)–(B4) show frequency distributions of S/$\bar{A}$ values for NR1, NR2A, and NR2B subunits. S/$\bar{A}$ > 1 indicates accumulation at silenced synapses.

(C) Across neurons, silenced synapses contained nearly 2-fold more NR1 and NR2B but similar levels of NR2A compared to active synapses. **$p < 0.01$.

(D) Homosynaptic accumulation of NR1 at silenced synapses. Shown is the spatial profile of NR1 accumulation at the nearest proximal (P) and distal (D) synapses in a 30 µm long stretch of dendrite centered by a single silenced synapse. NR1 accumulation is spatially confined to single silenced synapses. S/$\bar{A}$: silenced, 1.8 ± 0.2; P1, 1.1 ± 0.1; P2, 1.1 ± 0.1; P3, 1.2 ± 0.1; D1, 1.0 ± 0.1; D2, 0.8 ± 0.1; D3, 1.1 ± 0.1; n = 10 neurons. $p_{s-\bar{A}} < 0.01$ for comparisons between single silenced synapse and its neighboring active synapses; paired t test.

(E) Inactivity-induced accumulation of NR2B is homosynaptic. Analysis as in (D). S/$\bar{A}$: silenced, 2.1 ± 0.2; P1, 1.1 ± 0.2; P2, 0.9 ± 0.3; P3, 1.1 ± 0.3; D1, 1.1 ± 0.2; D2, 0.9 ± 0.1; D3, 1.1 ± 0.4; n = 18 neurons. $p_{s-\bar{A}} < 0.01$ for comparisons between single silenced synapse and its neighboring active synapses; paired t test.

glutamate receptors using the NMDAR antagonist D-AP5 and the AMPAR antagonist NBQX (Figure 3A). By blocking action potentials, addition of TTX abrogates evoked release, leaving only spontaneous release at active synapses (Figure 3A). Surprisingly, chronic TTX application had no effect on the accumulation of NR1 and NR2B at TeNT-silenced synapses (Figures 3B–3D, compare to Figure 2C). TTX had no effect whether applied 4 days after TeNT infection for 72 hr, or applied continuously for 7 days after TeNT infection (Figure S3A), indicating that action potentials are not required for inducing or maintaining NR1/NR2B receptors at silenced synapses. On the other hand, blockade of NMDARs by chronic D-AP5 application prevented the preferential accumulation of NR1 and NR2B at silenced synapses (Figures 3B–3D), thereby equalizing NMDAR content at silenced and active synapses. D-AP5 abolished the differential accumulation of NR1/NR2B at silenced synapses both when applied 4 days after TeNT infection for 72 hr, and when applied continuously for 7 days after TeNT infection (Figure S3B), indicating that ongoing NMDAR activation mediates the synapse-specific loss of NR1/NR2B at active synapses. Consistent with this notion, quantitative analysis revealed that the normalizing effect of AP5 was due to the global upregulation of NR1 and NR2B at nonsilenced synapses (Figure S3B). Thus, relative differences in NMDAR activity bidirectionally tune NR1/NR2B abundance. NR2A levels at active and silenced synapses were unchanged under all conditions (Figures 3E and S3C). Moreover, prolonged application of the AMPAR antagonist NBQX did not influence NR1/NR2B accumulation at silenced synapses (Figure S3C), indicating a selective effect of NMDAR activation.

To determine the time course and reversibility of this local activity-dependent NMDAR switch, synaptic levels of NR1 and

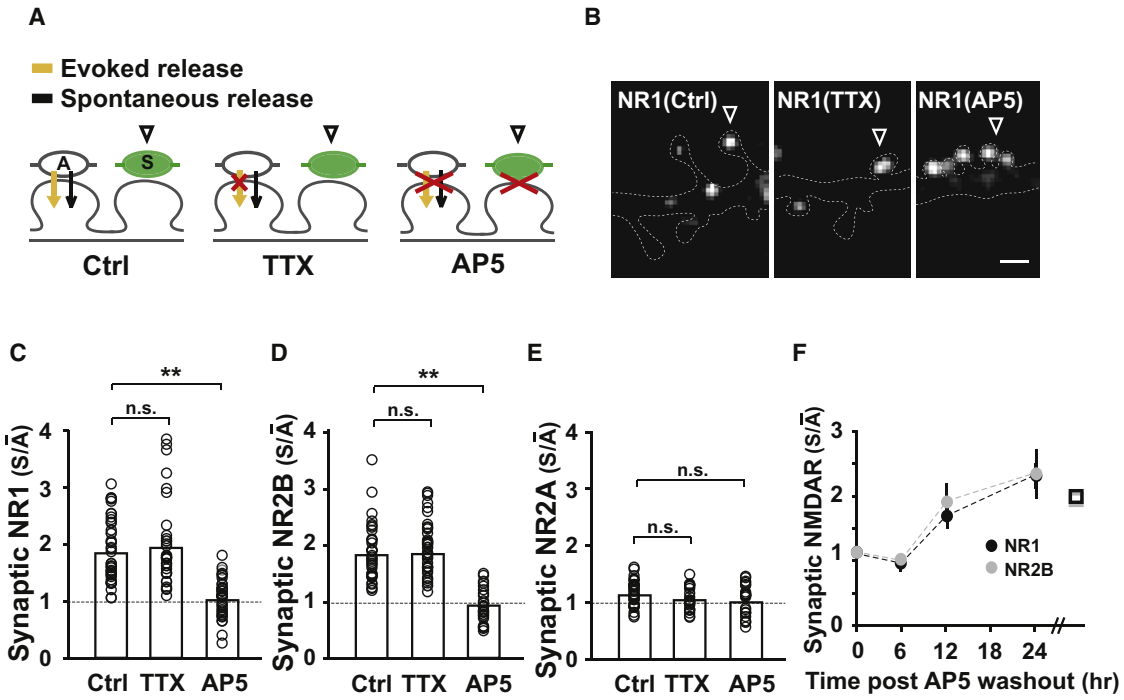

Figure 3. Local Spontaneous Release Determines NMDAR Content

(A) Schematic diagram indicating how specific manipulations affect action potential (AP)-evoked and spontaneous (or miniature) glutamate release at single active (A) and TeNT-silenced (S) synapses.

(B) Spontaneous glutamate release is sufficient to reduce NMDAR content at active synapses. Postsynaptic neurons contacted by active and TeNT-silenced (arrowheads) boutons were kept in the presence of TTX, AP5, or control solution for several days prior to fixation and immunolabeling for NR1 (see Experimental Procedures for details). Scale bar, 1 μm.

(C–E) Quantitative analyses of NMDAR accumulation at TeNT-silenced synapses. The relative accumulation of NR1 (C), NR2B (D), and NR2A (E) at silenced synapses (S/$\bar{A}$) was measured as in Figure 2 after prolonged treatment with TTX, AP5, or control (Ctrl) solution. Since both 3 and 7 days of pharmacological blockade resulted in similar effects on synaptic NMDAR accumulation (Figure S2C), pooled data are represented here. **$p < 0.01$. n.s., not significant.

(F) The time course of NR1/NR2B accumulation was monitored upon AP5 washout. Postsynaptic neurons contacted by active and TeNT-silenced boutons were incubated in TTX/AP5 medium for 3 days to equalize NMDAR content and then switched to TTX only medium for 6, 12, or 24 hr prior to fixation and immunostaining for NR1 and NR2B. The relative abundance of NR1 (black) and NR2B (gray) at silenced synapses relative to active synapses (S/$\bar{A}$) was measured over 24 hr. Data points at far right (squared) indicate S/$\bar{A}$ values under chronic TTX treatments derived from (C) and (D).

NR2B at active and silenced synapses were first equalized by 3 days of AP5 treatment and then tracked over time after AP5 washout in the continuous presence of TTX. After 3 days of AP5, S/$\bar{A}$ values for NR1 and NR2B were near 1.0 (Figure 3F), as expected (Figures 3C and 3D). After AP5 washout, S/$\bar{A}$ values for NR1 and NR2B slowly increased over 12–24 hr (Figure 3F), indicating that spontaneous activity mediates a reversible NMDAR switch over a time course of several hours.

Local Synaptic Activity Reduces Functional NR2B Content

The measured differences in NR2B protein levels at active and inactive synapses (Figures 2 and 3) suggest subunit-specific targeting as a mechanism for adjusting NMDAR currents on a synapse-by-synapse basis. To test this possibility, we measured the fractional contribution of NR2B-containing receptors to NMDAR currents recorded at active and silenced synapses. To isolate the contribution of NR2B, we used ifenprodil (3 μM), an NR2B-selective antagonist (Béïque et al., 2006; Bellone and Nicoll, 2007; Morishita et al., 2007; Sobczyk et al., 2005). Application of ifenprodil partially blocked NMDAR currents elicited by focal glutamate uncaging at active synapses (Figure 4A), consistent with a mixed population of NR2B-containing (ifenprodil-sensitive) and NR2B-lacking (ifenprodil-insensitive) receptors. The fraction of NR2B-containing NMDARs was then estimated by measuring ifenprodil sensitivity (Figures 4B–4F). At +40 mV, active synapses exhibited both a fast component mediated by AMPARs and a slow ifenprodil-resistant NMDAR component (Figure 4B, left). However, at silenced synapses, ifenprodil almost completely blocked the slow NMDAR current (Figure 4B, right). Comparison of averaged responses indicated a much larger inhibition of NMDAR currents by ifenprodil at silenced synapses (Figures 4C and 4E). Whereas active synapses had a sizeable residual NMDAR current in the presence of ifenprodil, very little ifenprodil-resistant NMDAR current remained at silenced synapses (Figures 4D and 4E). All residual NMDAR currents were completely blocked by the general NMDAR antagonist D-AP5 (data not shown), and AMPAR-uEPSCs measured at −70 mV were no different between the population of active and silenced synapses in the presence of ifenprodil

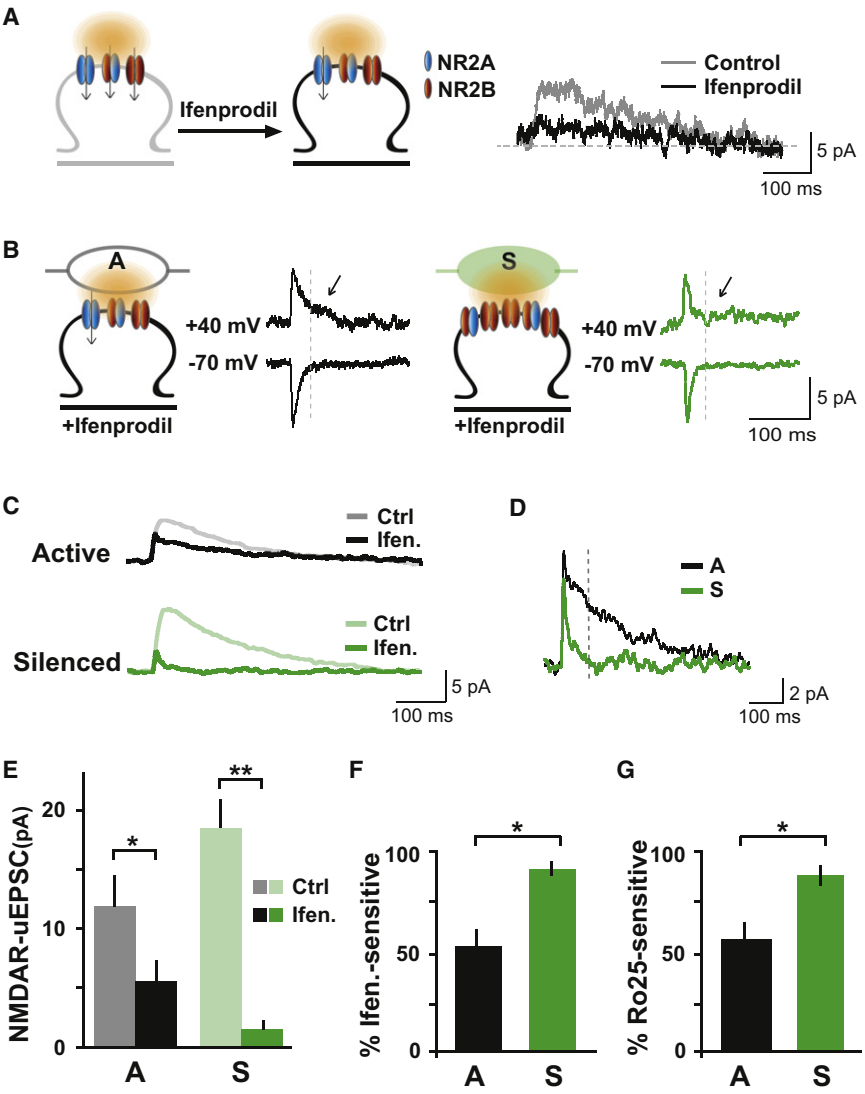

Figure 4. NR2B-Mediated Currents Dominate at Single Inactive Synapses

(A) Left, application of the selective NR2B antagonist ifenprodil allows estimation of the fractional contribution of NR2B-containing receptors to NMDAR currents elicited by focal two photon glutamate uncaging (orange spot) at single spines. Right, representative trace of NMDAR-uEPSCs measured before (control) and after ifenprodil application, indicating partial block.

(B) NMDAR currents at silenced synapses are more sensitive to ifenprodil. Shown are representative uEPSC traces recorded at −70 mV and + 40 mV in the presence of ifenprodil (3 μM) from one active synapse (A, left) and one silenced synapse (S, right). At the active synapse, $uEPSC_{+40mV}$ contained both a fast ifenprodil-resistant AMPAR-uEPSC and a slower ifenprodil-resistant NMDAR component (arrow). The silenced synapse contained an intact AMPAR-uEPSC but little ifenprodil-resistant NMDAR component (arrow).

(C) Average $uEPSC_{+40mV}$ traces from active (top) and silenced (bottom) synapses recorded with (Ifen.) or without (Ctrl) ifenprodil.

(D) Averaged ifenprodil-resistant $uEPSC_{+40mV}$ traces from active (A) and silenced (S) synapses.

(E) Data represent means ± SEM of NMDAR-uEPSCs at active (A) and silenced (S) synapses in the absence (Ctrl) or presence (Ifen.) of 3 μM ifenprodil. n = 12–26 synapses from 6–16 neurons for each condition. *p < 0.05, **p < 0.001.

(F) Percent ifenprodil sensitivity of NMDAR-uEPSCs recorded at active (A) and silenced (S) synapses. $*p_{A-S} < 0.05$.

(G) A second NR2B selective antagonist, Ro25-69821 (Ro25), has similar effects. Shown is the percent Ro25 sensitivity of NMDAR-uEPSCs recorded at active (A) and silenced (S) synapses. n = 7–26 synapses on 7–16 neurons for each condition. $*p_{A-S} < 0.05$.

(active, 8.7 ± 1.9 pA; silenced, 9.0 ± 1.2, p > 0.1). Quantitative analysis revealed that approximately half of the NMDAR current at active synapses was sensitive to ifenprodil, compared to > 90% at silenced synapses (Figure 4F; active, 52% ± 13% ifenprodil-sensitive; silenced 92% ± 3%; *p < 0.05). Similar results were obtained using another NR2B-selective blocker, Ro25-6981 (Figure 4G; active, 57% ± 9% Ro25-sensitive; silenced 88% ± 5%; *p < 0.05). These results indicate that local activity determines NMDAR subtype abundance and associated subunit-specific NMDAR currents at single synapses. Specifically, when the activity of a single synapse is reduced, the contribution of NR2B-containing NMDARs to synaptic transmission at that synapse is enhanced.

Silenced Synapses Have a Lower Threshold for Potentiation

We reasoned that the elevated levels of NR2B at silenced synapses might alter Ca^{2+} dynamics upon stimulation and thereby increase sensitivity to plasticity induction (Barria and Malinow, 2005; Gardoni et al., 2009; Jung et al., 2008; Tang et al., 1999; Yashiro and Philpot, 2008). We first performed Ca^{2+} imaging at nearby pairs of dendritic spines corresponding to active and silenced synapses (Figure 5A; see Experimental Procedures for details). In these experiments, neurons were patch loaded with a green (*G*) Ca^{2+}-sensitive fluorophore (Fluo-4FF) and a red (*R*) Ca^{2+}-insensitive fluorophore (Alexa-594). Ca^{2+} transients were recorded in 0 mM extracellular Mg^{2+} and in the presence of drugs that block AMPARs (10 μM NBQX) and Ca^{2+} release from internal stores (1 μM thapsigargin, 20 μM ryanodine). Uncaging-evoked Ca^{2+} transients were measured as the change in green fluorescence (ΔG) divided by red fluorescence (*R*), normalized to $(G/R)_{MAX}$ measured in 10 mM Ca^{2+} (Harvey and Svoboda, 2007; Yasuda et al., 2004). In response to local glutamate uncaging, silenced synapses exhibited a much larger Ca^{2+} transient compared to their active neighbors (Figure 5A). Ca^{2+} transients were largely limited to the stimulated spine, with only small rises in the adjacent dendritic shaft (Figure 5A). Quantitative analysis revealed that the peak $[Ca^{2+}]$ at spine heads was

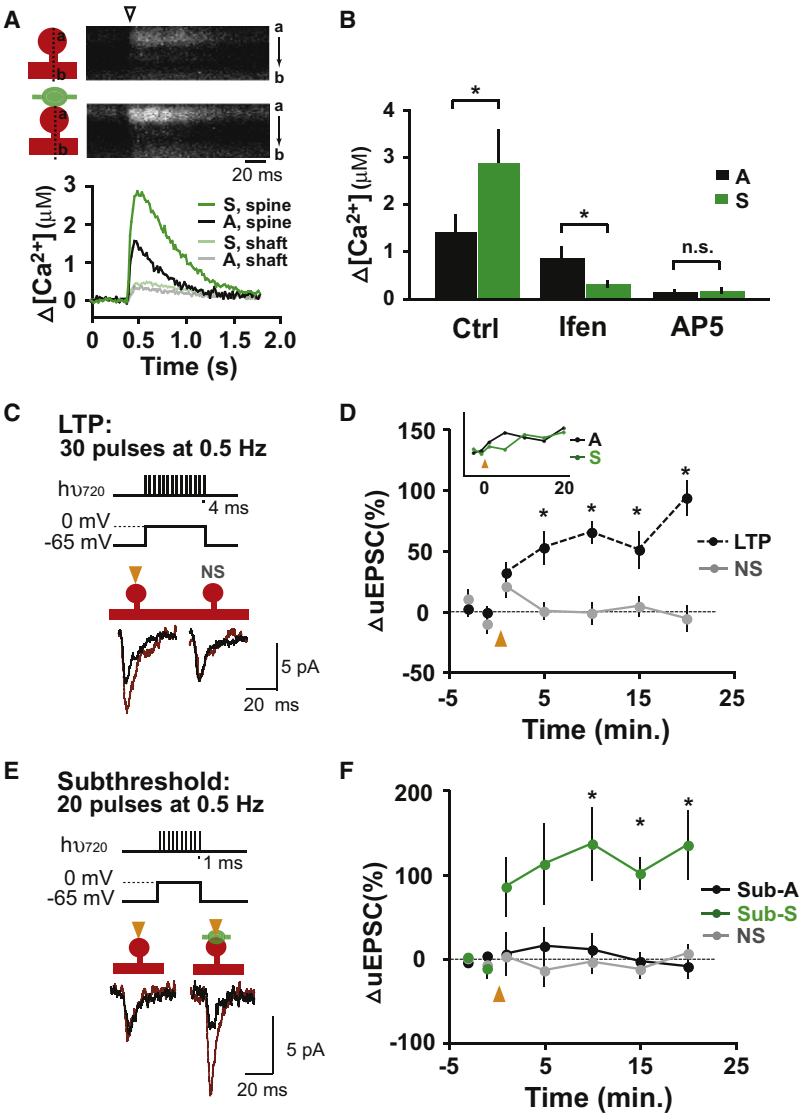

Figure 5. Prolonged Inactivation Primes Single Synapses for Potentiation

(A) Silenced synapses exhibit an elevated Ca^{2+} transient compared to their active neighbors. Upper panel, shown are representative kymographs of Fluo-4FF signal upon local glutamate uncaging (arrowhead) at nearby active (A) and silenced (S) synapses on dendritic spines. Lower panel, plotted is the average change in Ca^{2+} concentration over time following local glutamate uncaging. See Experimental Procedures for details.

(B) Data show means ± SEM of the peak change in Ca^{2+} concentration at active (A) and silenced (S) synapses under control conditions (Ctrl) or in the presence of ifenprodil (Ifen) or AP5. *$p < 0.05$; n = 8, 7, 4 pairs from 6, 6, 4 neurons, respectively; paired t test; n.s. not significant.

(C) Pairing-induced LTP at single synapses. By pairing 30 focal glutamate uncaging pulses of 4 ms duration with postsynaptic depolarization, LTP of AMPAR-uEPSCs was reliably induced at the stimulated spine (orange arrowheads, left traces), but not at the nonstimulated neighboring spine (NS, right traces). Current traces before (black) and after (red) conditioning stimuli are shown.

(D) Quantification of uEPSC potentiation following LTP induction. The potentiation of AMPAR-uEPSCs following a 30 pulse pairing LTP protocol persisted for more than 20 min (LTP, 193% ± 14% at 20 min post LTP induction, n = 13). The inset shows that the potentiation of active (A, black) and silenced (S, green) synapses was undistinguishable using the 30 pulse protocol ($p > 0.05$ for the last three time points shown). NS, nonstimulated neighboring spine. *$p < 0.05$.

(E) Weak stimuli potentiate silenced but not active synapses. A weaker stimulation protocol (subthreshold protocol: 20 pulses of 1 ms duration paired with 0 mV depolarization), failed to potentiate active synapses (left traces) but triggered a sustained potentiation at silenced synapses (right traces). Current traces before (black) and after (red) conditioning stimuli are shown.

(F) Quantification of uEPSC potentiation following subthreshold stimulation at active (Sub-A) and silenced (Sub-S) synapses compared to non-stimulated neighboring spines (NS). Active, 90% ± 13% at 20 min postinduction; silenced 235% ± 40%; n = 6, 9, respectively; NS, 106% ± 10%. *$p < 0.05$.

nearly twice as large at silenced synapses relative to neighboring active synapses ([Ca^{2+}] in μM: active, 1.4 ± 0.3; silenced, 2.9 ± 0.7; paired-t test, *$p < 0.05$; n = 8 pairs from 6 neurons; Figure 5B). Consistent with the ifenprodil sensitivity of recorded NMDAR currents (Figure 4), Ca^{2+} transients at silenced spines were more strongly blocked by ifenprodil than neighboring active spines ([Ca^{2+}] in μM: Ifen active, 0.88 ± 0.2; Ifen silenced, 0.32 ± 0.6; AP5 active, 0.17 ± 0.3; AP5 silenced, 0.15 ± 0.4; Figure 5B).

Larger Ca^{2+} transients in spines are associated with synaptic potentiation (Cormier et al., 2001; Zucker, 1999). To determine whether changes in NMDARs at silenced synapses lead to a reduced plasticity threshold, we used two-photon glutamate uncaging to induce long-term potentiation (LTP) of AMPAR-uEPSCs at individual silenced and active synapses. In order to reliably potentiate AMPAR-uEPSCs, repetitive glutamate uncaging stimulation was paired with postsynaptic depolarization (LTP protocol: 30 pulses of 4 ms duration at 0.5 Hz paired with postsynaptic depolarization to 0 mV; Figure 5C). For each experiment, two nearby dendritic spines were selected, pairing a target spine (either active or silenced) with a nonstimulated neighboring spine (NS). While target spines were subjected to repetitive uncaging stimuli, nonstimulated spines served as controls. The potentiation of AMPAR-uEPSCs at stimulated synapses persisted for more than 20 min (Figure 5D; 193% ± 14% at 20 min post LTP induction) while AMPAR-uEPSCs at nonstimulated spines were unchanged (94% ± 10%). With the 30 pulse protocol, LTP was indistinguishable between active and silenced synapses ($p > 0.05$ for the last 3 time points shown in Figure 5D inset), indicating that both active and silenced synapses are capable of being potentiated by strong stimulation. In contrast to the robust potentiation with the 30 pulse protocol (Figure 5D), active synapses were not potentiated by a weaker stimulation protocol consisting of 20 pulses of 1 ms duration at 0.5 Hz paired with postsynaptic depolarization at 0 mV (90% ± 13% at 20 min post-stimulation; Figures 5E and 5F). Yet, this subthreshold protocol reliably induced LTP at silenced synapses

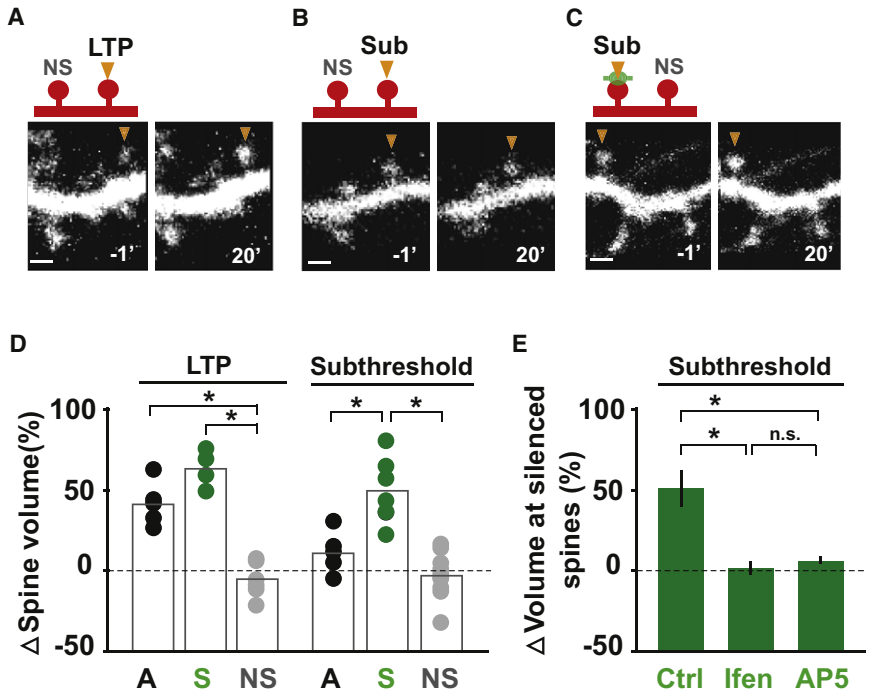

Figure 6. Subthreshold Stimuli Elicit Plasticity-Induced Spine Growth at Silenced Synapses

(A) LTP induction by two-photon glutamate uncaging (LTP, 30 pulses of 4 ms duration at 0.5 Hz in 0 Mg^{2+}) triggers sustained spine growth at active synapses. For (A)–(C), time is indicated in minutes. NS, nonstimulated neighboring spine. Scale bar, 1 μm.

(B) A weaker subthreshold stimulus (Sub) consisting of 20 glutamate uncaging pulses of 1 ms duration at 0.5 Hz in 0 Mg^{2+} does not elicit spine growth at active synapses.

(C) The normally subthreshold protocol of 20 focal glutamate uncaging pulses of 1 ms duration (Sub, arrowhead) elicits robust spine growth at silenced (green bouton) synapses.

(D) Quantitative analysis of spine volume change following a strong LTP protocol (30 pulse, 4 ms) or a subthreshold stimulus (20 pulses, 1 ms). All trials are shown. Bars indicate means. A, active synapse; S, silenced synapse; NS, nonstimulated synapse. 30 pulses: $*p_{A\text{-}NS} < 0.01$, $*p_{S\text{-}NS} < 0.01$, $p_{A\text{-}S} > 0.1$; 20 pulses: $p_{A\text{-}NS} > 0.1$, $*p_{S\text{-}NS} < 0.01$, $*p_{A\text{-}S} < 0.05$.

(E) Spine growth at silenced synapses elicited by subthreshold stimuli requires NR2B-containing NMDARs. In the presence of ifenprodil (Ifen.) or AP5, the subthreshold protocol failed to induce spine enlargement at silenced synapses. Ctrl, 151% ± 11% at 20 min postinduction; Ifen., 101% ± 3%; AP5, 104% ± 2%; n = 6, 7, 4, respectively; $*p < 0.05$. n.s., not significant.

(Figure 5F; 235% ± 40% at 20 min post-stimulation). These data show that prolonged inactivation primes individual synapses for potentiation, providing direct evidence for metaplasticity at single synapses.

Local Synaptic Activity Suppresses Plasticity-Induced Spine Growth

At hippocampal synapses, single synapse potentiation by focal glutamate uncaging is accompanied by structural plasticity, most notably growth of activated dendritic spines (Harvey and Svoboda, 2007; Harvey et al., 2008; Lee et al., 2009; Matsuzaki et al., 2004). To test whether plasticity-induced growth of a given dendritic spine is regulated by its previous history of activity, we measured stimulus-induced spine enlargement at single silenced and active synapses. Single dendritic spines were stimulated by focal glutamate uncaging and spine volume was monitored by measuring fluorescence intensity changes of mCherry expressed as a cell fill (see Experimental Procedures for details). An LTP protocol was applied (30 pulses of 4 ms duration at 0.5 Hz, 0 Mg^{2+}) to induce a sustained increase in spine volume at stimulated synapses (Figure S4). Following uncaging stimulation, active synapses showed prolonged spine enlargement after the LTP protocol (Figure 6A) but exhibited no spine growth in response to a weaker subthreshold protocol (Figure 6B; 20 pulses of 1 ms duration at 0.5 Hz, 0 Mg^{2+}). However, both protocols triggered sustained spine enlargement at silenced synapses (Figures 6C and 6D; active 30 pulse, 142% ± 9% spine growth; active 20 pulse, 112% ± 9%; silenced 30 pulse, 162% ± 8%; silenced 20 pulse, 143% ± 9%). Addition of either ifenprodil or AP5 blocked spine enlargement at silenced synapses induced by the subthreshold protocol (Figure 6E), indicating that this sensitized spine growth requires activation of NR2B-containing NMDARs. Thus, local activity sets the threshold for both functional and structural plasticity on a synapse-by-synapse basis, defining a spatially delimited form of synaptic metaplasticity.

DISCUSSION

In this study, we have shown that prior activity determines the propensity for plasticity at single synapses. Prolonged suppression of activity triggers the accumulation of NR2B-containing NMDARs at single synapses, which allows larger Ca^{2+} transients and in turn primes synapses for potentiation. Conversely, neighboring active synapses have fewer NMDARs, less NR2B, smaller Ca^{2+} transients, and exhibit higher thresholds for potentiation. Remarkably, spontaneous miniature release is sufficient to induce local changes in NMDAR composition. These results reveal a novel mechanistic basis and single synapse length scale for metaplasticity.

Modifying NMDAR Composition at Single Synapses

The relative abundance of NR2A and NR2B is a well-established determinant of synaptic and developmental plasticity in diverse brain circuits (Yashiro and Philpot, 2008). The NR2A/NR2B ratio changes with development (Barria and Malinow, 2002; Liu et al., 2004b; Sheng et al., 1994), sensory experience (Carmignoto and Vicini, 1992; Hestrin, 1992; Quinlan et al., 1999), and synaptic

plasticity (Bellone and Nicoll, 2007). Most studies that have addressed the regulation of NR2 composition have employed global manipulations of activity, such as chronic treatment with NMDAR antagonists (Barria and Malinow, 2002; Groc et al., 2006) or dark-rearing (Chen et al., 2000; Yashiro et al., 2005). However, NR2A/NR2B ratios differ between distinct sets of synapses onto single neurons (Arrigoni and Greene, 2004; Ito et al., 1997, 2000; Kawakami et al., 2003; Kumar and Huguenard, 2003; Wu et al., 2005). How such differences in NMDAR composition arise, and whether NMDAR composition represents an intrinsic quality of specific synapses or is subject to ongoing regulation is unclear. In support of the latter, NMDAR currents scale up proportionally with AMPAR currents both upon global activity blockade (Watt et al., 2000) and, with a delay, following LTP induction (Watt et al., 2004). In addition, LTP-inducing stimuli in young CA1 hippocampus produce a rapid reversible switch from NR2B to NR2A (Bellone and Nicoll, 2007). However, whether such changes occur at single synapses, and what the functional consequences are for plasticity induction have been unknown. We addressed this problem through selective genetic inactivation of sparse defined inputs onto individual postsynaptic neurons coupled with focal two-photon glutamate uncaging. This approach allowed us to measure NMDAR composition and function at single synapses, and determine the consequences for plasticity induction.

Our results indicate that silenced synapses possess a higher fraction of NR2B-containing NMDARs, likely including both triheteromeric (NR1/NR2A/NR2B) and diheteromeric (NR1/NR2B) receptors. Input-specific regulation of NMDAR composition by ongoing local activity may help explain the heterogeneous expression of NR2B-containing receptors observed across hippocampal CA1 synapses (Sobczyk et al., 2005) and may account for the afferent-specific NMDAR composition observed in hippocampal neurons and cortical neurons (Arrigoni and Greene, 2004; Ito et al., 1997, 2000; Kawakami et al., 2003; Kumar and Huguenard, 2003; Wu et al., 2005). It is perhaps surprising that AMPAR currents are unaltered at inactive synapses. It is possible that AMPARs are lost at later time points (e.g., after several weeks) or that changes in AMPAR subtype that alter channel conductance (e.g., GluR2-containing versus GluR2-lacking) produce compensating changes in AMPAR currents despite reduced receptor number (Liu and Cull-Candy, 2005; Mameli et al., 2007).

Spatial Tuning of NMDAR-Dependent Plasticity

It is well established that synaptic NMDAR composition influences the induction of synaptic plasticity (Barria and Malinow, 2005; Gardoni et al., 2009; Jung et al., 2008; Liu et al., 2004a; Tang et al., 1999). Yet, the spatial scales of NMDAR compositional changes and the precise role of specific receptor subunits are controversial (Barria and Malinow, 2005; Jung et al., 2008; Liu et al., 2004a; Massey et al., 2004; Morishita et al., 2007; Philpot et al., 2007; Tang et al., 1999; Zhou et al., 2007). A prevailing model suggests that the relative levels of NR2A and NR2B modify the threshold for LTP and LTD induction (Kopp et al., 2006; Philpot et al., 2007; Yashiro and Philpot, 2008). Here, by functionally suppressing individual synaptic inputs, we uncovered a profound synapse-specific decrease in LTP induction threshold associated with homosynaptically elevated NR2B and increased spine Ca^{2+} accumulation. The increase in Ca^{2+} entry could plausibly account for a lower threshold for LTP induction (Lisman et al., 2002; Lisman, 2001). Moreover, the strong interaction between NR2B and CaMKII (Barria and Malinow, 2005; Bayer et al., 2001) may also lower plasticity threshold by localizing key signaling molecules in proximity to the NMDAR at single synapses (Barria and Malinow, 2005; Yashiro and Philpot, 2008; Zhou et al., 2007).

Spontaneous Glutamate Release as a Cue for Input-Specific Metaplasticity

In the presence of TTX to block action potentials, the suppression of spontaneous (or miniature) release at individual TeNT-expressing boutons allowed us to determine how ongoing spontaneous release modifies synaptic composition and signaling at single synapses. While spontaneous release has been previously reported to regulate postsynaptic AMPAR scaling (Sutton et al., 2004), our work shows that synapses with lower rates of spontaneous release become more easily potentiated. The notion that spontaneous release can induce input-specific metaplasticity is consistent with observations that glutamate binding to NMDARs facilitates the developmental switch from NR2B to NR2A in a cell-wide manner (Barria and Malinow, 2002). Manipulations that reduce action potential-induced release, but not miniature release, increase GluR1 AMPARs at single synapses (Hou et al., 2008), whereas suppressing both forms of release causes GluR1 loss (Ehlers et al., 2007; Harms and Craig, 2005), further documenting selective effects of spontaneous glutamate release. Moreover, evoked and spontaneous release events have been found to originate from separate presynaptic vesicle pools and may be detected by distinct pools of postsynaptic NMDARs (Atasoy et al., 2008; Fredj and Burrone, 2009; Sara et al., 2005), raising the possibility that evoked and spontaneous release are independently regulated and represent distinct modes of postsynaptic signaling.

Spontaneous release is not generally considered as an adjustable parameter for information encoding, but recent studies indicate that the frequency of spontaneous release can be regulated by the activity state of individual cells (Murthy et al., 2001; Nelson et al., 2006, 2008). Together with our findings, this suggests that spontaneous release is a tunable input-specific signature that plays a distinct role in receptor accumulation and postsynaptic plasticity. Changes in spontaneous release may provide a general mechanism to dynamically adjust plasticity threshold in an input-specific manner. Thus, at single synapses the threshold for plasticity may not only be heterosynaptically influenced by evoked activity (Harvey and Svoboda, 2007), but also homosynaptically modified by the rate of tonic spontaneous release to express variation in the form, magnitude, and propensity for plasticity.

We propose that by providing spatially delimited control over NMDAR number and composition, local increases or decreases in synaptic activity alternately dampen or prime long-term synaptic potentiation. This negative feedback of NMDAR-dependent plasticity provides a potential synaptic basis for augmenting or accentuating salient activity in noisy networks. Such a mechanism may provide a general paradigm for optimizing

activity-dependent gain control and stimulus selection in diverse neural circuits.

EXPERIMENTAL PROCEDURES

DNA Constructs and Reagents

Synaptophysin-EGFP was kindly provided by George Augustine (Duke University, Durham, NC). Tetanus toxin light chain (TeNT-LC) cDNA was a gift from Joseph Gogos (Columbia University, New York, NY). These two cDNAs were cloned in frame before and after the internal ribosome entry site (IRES) of pIRES-EGFP (Clontech), respectively. Synaptophysin-EGFP-IRES-TeNTlc (SphGFP-IRES-TeNT) was incorporated into a lentiviral expression vector (Transzyme, Durham, NC) to generate high titer virus (0.1 – 1.0 × 10^9 particles/ml).

Image and Image Analysis

For fixed samples, images were acquired using an Ultraview spinning disc confocal microscope (Perkin Elmer Inc.) and analyzed using Metamorph (Universal Imaging Corporation). Dendrites were traced using an expressed mCherry cell fill. Maximum projections of z series (0.5 μm steps) were used for quantification of synaptic NMDAR contents.

Further details are provided in the Supplemental Experimental Procedures online.

Two-Photon Microscopy and Electrophysiology

Two-photon laser-scanning microscopy and two-photon glutamate uncaging were performed on a custom imaging system using two Ti:sapphire pulsed lasers (MaiTai, Spectra-Physics, Fremont, CA), which were tuned to 920 nm for imaging and 720 nm for glutamate uncaging. The intensity of each laser beam was independently controlled with electro-optical modulators (350-80 LA; Conoptics, Danbury, CT). Beams were combined using a dichroic mirror (790SP; Chroma Technology, Brattleboro, VT) and traversed the same set of scan mirrors and a 60×, 0.9 NA objective (Olympus, Melville, NY). Fluorescence was detected by summing epifluorescence and transfluorescence signals as described previously (Mainen et al., 1999). All two-photon experiments were performed at room temperature in ACSF containing the following (in mM): 2.0 $MgCl_2$, 2.0 $CaCl_2$, 0.002 TTX and 2.0 4-methoxy-7-nitroindolinyl (MNI)-caged-L-glutamate except for the spine enlargement and Ca^{2+} imaging assays where 0 $MgCl_2$ was applied. ACSF was constantly bubbled with 95% O_2 and 5% CO_2 throughout the experiment. MNI-caged L-glutamate and TTX were from Tocris Cookson (Ballwin, MO). Imaged and stimulated spines were located on secondary and tertiary apical dendrites within 150 μm of the soma.

Detailed protocols of calcium imaging and plasticity induction are provided in the Supplemental Experimental Procedures online.

SUPPLEMENTAL INFORMATION

Supplemental Information includes four figures and Supplemental Experimental Procedures and can be found with this article online at doi:10.1016/j.neuron.2010.05.015.

ACKNOWLEDGMENTS

We thank Benjamin Arenkiel, Ian Davison, David Fitzpatrick, Juliet Hernandez, Matt Kennedy, Shih-Chieh Lin, Tom Newpher, Sri Raghavachari, and Richard Weinberg for critical review of the manuscript. We thank Irina Lebedeva and Marguerita Klein for excellent technical assistance. This work was supported by grants from the NINDS/NIH and NIMH/NIH to M.D.E. and NIMH/NIH to R.Y. M.D.E. is an Investigator of the Howard Hughes Medical Institute. R.Y. is an Early Career Scientist of the Howard Hughes Medical Institute.

Accepted: May 12, 2010
Published: June 23, 2010

REFERENCES

Abraham, W.C. (2008). Metaplasticity: tuning synapses and networks for plasticity. Nat. Rev. Neurosci. *9*, 387.

Arrigoni, E., and Greene, R.W. (2004). Schaffer collateral and perforant path inputs activate different subtypes of NMDA receptors on the same CA1 pyramidal cell. Br. J. Pharmacol. *142*, 317–322.

Atasoy, D., Ertunc, M., Moulder, K.L., Blackwell, J., Chung, C., Su, J., and Kavalali, E.T. (2008). Spontaneous and evoked glutamate release activates two populations of NMDA receptors with limited overlap. J. Neurosci. *28*, 10151–10166.

Barria, A., and Malinow, R. (2002). Subunit-specific NMDA receptor trafficking to synapses. Neuron *35*, 345–353.

Barria, A., and Malinow, R. (2005). NMDA receptor subunit composition controls synaptic plasticity by regulating binding to CaMKII. Neuron *48*, 289–301.

Bayer, K.U., De Koninck, P., Leonard, A.S., Hell, J.W., and Schulman, H. (2001). Interaction with the NMDA receptor locks CaMKII in an active conformation. Nature *411*, 801–805.

Béïque, J.C., Lin, D.T., Kang, M.G., Aizawa, H., Takamiya, K., and Huganir, R.L. (2006). Synapse-specific regulation of AMPA receptor function by PSD-95. Proc. Natl. Acad. Sci. USA *103*, 19535–19540.

Bellone, C., and Nicoll, R.A. (2007). Rapid bidirectional switching of synaptic NMDA receptors. Neuron *55*, 779–785.

Capogna, M., McKinney, R.A., O'Connor, V., Gähwiler, B.H., and Thompson, S.M. (1997). Ca2+ or Sr2+ partially rescues synaptic transmission in hippocampal cultures treated with botulinum toxin A and C, but not tetanus toxin. J. Neurosci. *17*, 7190–7202.

Carmignoto, G., and Vicini, S. (1992). Activity-dependent decrease in NMDA receptor responses during development of the visual cortex. Science *258*, 1007–1011.

Chen, L., Cooper, N.G., and Mower, G.D. (2000). Developmental changes in the expression of NMDA receptor subunits (NR1, NR2A, NR2B) in the cat visual cortex and the effects of dark rearing. Brain Res. Mol. Brain Res. *78*, 196–200.

Colonnese, M.T., Shi, J., and Constantine-Paton, M. (2003). Chronic NMDA receptor blockade from birth delays the maturation of NMDA currents, but does not affect AMPA/kainate currents. J. Neurophysiol. *89*, 57–68.

Cormier, R.J., Greenwood, A.C., and Connor, J.A. (2001). Bidirectional synaptic plasticity correlated with the magnitude of dendritic calcium transients above a threshold. J. Neurophysiol. *85*, 399–406.

Cull-Candy, S.G., and Leszkiewicz, D.N. (2004). Role of distinct NMDA receptor subtypes at central synapses. Sci. STKE *2004*, re16.

Ehlers, M.D., Zhang, S., Bernhadt, J.P., and Huganir, R.L. (1996). Inactivation of NMDA receptors by direct interaction of calmodulin with the NR1 subunit. Cell *84*, 745–755.

Ehlers, M.D., Heine, M., Groc, L., Lee, M.C., and Choquet, D. (2007). Diffusional trapping of GluR1 AMPA receptors by input-specific synaptic activity. Neuron *54*, 447–460.

Erreger, K., Dravid, S.M., Banke, T.G., Wyllie, D.J., and Traynelis, S.F. (2005). Subunit-specific gating controls rat NR1/NR2A and NR1/NR2B NMDA channel kinetics and synaptic signalling profiles. J. Physiol. *563*, 345–358.

Foster, K.A., McLaughlin, N., Edbauer, D., Phillips, M., Bolton, A., Constantine-Paton, M., and Sheng, M. (2010). Distinct roles of NR2A and NR2B cytoplasmic tails in long-term potentiation. J. Neurosci. *30*, 2676–2685.

Fredj, N.B., and Burrone, J. (2009). A resting pool of vesicles is responsible for spontaneous vesicle fusion at the synapse. Nat. Neurosci. *12*, 751–758.

Fusi, S., and Abbott, L.F. (2007). Limits on the memory storage capacity of bounded synapses. Nat. Neurosci. *10*, 485–493.

Fusi, S., Drew, P.J., and Abbott, L.F. (2005). Cascade models of synaptically stored memories. Neuron *45*, 599–611.

Gardoni, F., Mauceri, D., Malinverno, M., Polli, F., Costa, C., Tozzi, A., Siliquini, S., Picconi, B., Cattabeni, F., Calabresi, P., and Di Luca, M. (2009). Decreased

NR2B subunit synaptic levels cause impaired long-term potentiation but not long-term depression. J. Neurosci. *29*, 669–677.

Groc, L., Heine, M., Cousins, S.L., Stephenson, F.A., Lounis, B., Cognet, L., and Choquet, D. (2006). NMDA receptor surface mobility depends on NR2A-2B subunits. Proc. Natl. Acad. Sci. USA *103*, 18769–18774.

Harms, K.J., and Craig, A.M. (2005). Synapse composition and organization following chronic activity blockade in cultured hippocampal neurons. J. Comp. Neurol. *490*, 72–84.

Harms, K.J., Tovar, K.R., and Craig, A.M. (2005). Synapse-specific regulation of AMPA receptor subunit composition by activity. J. Neurosci. *25*, 6379–6388.

Harvey, C.D., and Svoboda, K. (2007). Locally dynamic synaptic learning rules in pyramidal neuron dendrites. Nature *450*, 1195–1200.

Harvey, C.D., Yasuda, R., Zhong, H., and Svoboda, K. (2008). The spread of Ras activity triggered by activation of a single dendritic spine. Science *321*, 136–140.

Hestrin, S. (1992). Developmental regulation of NMDA receptor-mediated synaptic currents at a central synapse. Nature *357*, 686–689.

Hoffmann, H., Gremme, T., Hatt, H., and Gottmann, K. (2000). Synaptic activity-dependent developmental regulation of NMDA receptor subunit expression in cultured neocortical neurons. J. Neurochem. *75*, 1590–1599.

Hou, Q., Zhang, D., Jarzylo, L., Huganir, R.L., and Man, H.Y. (2008). Homeostatic regulation of AMPA receptor expression at single hippocampal synapses. Proc. Natl. Acad. Sci. USA *105*, 775–780.

Ito, I., Futai, K., Katagiri, H., Watanabe, M., Sakimura, K., Mishina, M., and Sugiyama, H. (1997). Synapse-selective impairment of NMDA receptor functions in mice lacking NMDA receptor epsilon 1 or epsilon 2 subunit. J. Physiol. *500*, 401–408.

Ito, I., Kawakami, R., Sakimura, K., Mishina, M., and Sugiyama, H. (2000). Input-specific targeting of NMDA receptor subtypes at mouse hippocampal CA3 pyramidal neuron synapses. Neuropharmacology *39*, 943–951.

Jung, S.C., Kim, J., and Hoffman, D.A. (2008). Rapid, bidirectional remodeling of synaptic NMDA receptor subunit composition by A-type K+ channel activity in hippocampal CA1 pyramidal neurons. Neuron *60*, 657–671.

Kawakami, R., Shinohara, Y., Kato, Y., Sugiyama, H., Shigemoto, R., and Ito, I. (2003). Asymmetrical allocation of NMDA receptor epsilon2 subunits in hippocampal circuitry. Science *300*, 990–994.

Kessels, H.W., and Malinow, R. (2009). Synaptic AMPA receptor plasticity and behavior. Neuron *61*, 340–350.

Kim, M.J., Dunah, A.W., Wang, Y.T., and Sheng, M. (2005). Differential roles of NR2A- and NR2B-containing NMDA receptors in Ras-ERK signaling and AMPA receptor trafficking. Neuron *46*, 745–760.

Kopp, C., Longordo, F., Nicholson, J.R., and Lüthi, A. (2006). Insufficient sleep reversibly alters bidirectional synaptic plasticity and NMDA receptor function. J. Neurosci. *26*, 12456–12465.

Kumar, S.S., and Huguenard, J.R. (2003). Pathway-specific differences in subunit composition of synaptic NMDA receptors on pyramidal neurons in neocortex. J. Neurosci. *23*, 10074–10083.

Lau, C.G., and Zukin, R.S. (2007). NMDA receptor trafficking in synaptic plasticity and neuropsychiatric disorders. Nat. Rev. Neurosci. *8*, 413–426.

Lee, S.J., Escobedo-Lozoya, Y., Szatmari, E.M., and Yasuda, R. (2009). Activation of CaMKII in single dendritic spines during long-term potentiation. Nature *458*, 299–304.

Lisman, J.E. (2001). Three Ca2+ levels affect plasticity differently: the LTP zone, the LTD zone and no man's land. J. Physiol. *532*, 285.

Lisman, J., Schulman, H., and Cline, H. (2002). The molecular basis of CaMKII function in synaptic and behavioural memory. Nat. Rev. Neurosci. *3*, 175–190.

Liu, S.J., and Cull-Candy, S.G. (2005). Subunit interaction with PICK and GRIP controls Ca2+ permeability of AMPARs at cerebellar synapses. Nat. Neurosci. *8*, 768–775.

Liu, L., Wong, T.P., Pozza, M.F., Lingenhoehl, K., Wang, Y., Sheng, M., Auberson, Y.P., and Wang, Y.T. (2004a). Role of NMDA receptor subtypes in governing the direction of hippocampal synaptic plasticity. Science *304*, 1021–1024.

Liu, X.B., Murray, K.D., and Jones, E.G. (2004b). Switching of NMDA receptor 2A and 2B subunits at thalamic and cortical synapses during early postnatal development. J. Neurosci. *24*, 8885–8895.

Mainen, Z.F., Maletic-Savatic, M., Shi, S.H., Hayashi, Y., Malinow, R., and Svoboda, K. (1999). Two-photon imaging in living brain slices. Methods *18*, 231–239.

Malenka, R.C., and Bear, M.F. (2004). LTP and LTD: an embarrassment of riches. Neuron *44*, 5–21.

Mameli, M., Balland, B., Luján, R., and Lüscher, C. (2007). Rapid synthesis and synaptic insertion of GluR2 for mGluR-LTD in the ventral tegmental area. Science *317*, 530–533.

Massey, P.V., Johnson, B.E., Moult, P.R., Auberson, Y.P., Brown, M.W., Molnar, E., Collingridge, G.L., and Bashir, Z.I. (2004). Differential roles of NR2A and NR2B-containing NMDA receptors in cortical long-term potentiation and long-term depression. J. Neurosci. *24*, 7821–7828.

Matsuzaki, M., Honkura, N., Ellis-Davies, G.C., and Kasai, H. (2004). Structural basis of long-term potentiation in single dendritic spines. Nature *429*, 761–766.

Montgomery, J.M., and Madison, D.V. (2002). State-dependent heterogeneity in synaptic depression between pyramidal cell pairs. Neuron *33*, 765–777.

Monyer, H., Burnashev, N., Laurie, D.J., Sakmann, B., and Seeburg, P.H. (1994). Developmental and regional expression in the rat brain and functional properties of four NMDA receptors. Neuron *12*, 529–540.

Morishita, W., Lu, W., Smith, G.B., Nicoll, R.A., Bear, M.F., and Malenka, R.C. (2007). Activation of NR2B-containing NMDA receptors is not required for NMDA receptor-dependent long-term depression. Neuropharmacology *52*, 71–76.

Mu, Y., Otsuka, T., Horton, A.C., Scott, D.B., and Ehlers, M.D. (2003). Activity-dependent mRNA splicing controls ER export and synaptic delivery of NMDA receptors. Neuron *40*, 581–594.

Murthy, V.N., Schikorski, T., Stevens, C.F., and Zhu, Y. (2001). Inactivity produces increases in neurotransmitter release and synapse size. Neuron *32*, 673–682.

Nelson, E.D., Kavalali, E.T., and Monteggia, L.M. (2006). MeCP2-dependent transcriptional repression regulates excitatory neurotransmission. Curr. Biol. *16*, 710–716.

Nelson, E.D., Kavalali, E.T., and Monteggia, L.M. (2008). Activity-dependent suppression of miniature neurotransmission through the regulation of DNA methylation. J. Neurosci. *28*, 395–406.

Newpher, T.M., and Ehlers, M.D. (2008). Glutamate receptor dynamics in dendritic microdomains. Neuron *58*, 472–497.

Philpot, B.D., Cho, K.K., and Bear, M.F. (2007). Obligatory role of NR2A for metaplasticity in visual cortex. Neuron *53*, 495–502.

Poncer, J.C., and Malinow, R. (2001). Postsynaptic conversion of silent synapses during LTP affects synaptic gain and transmission dynamics. Nat. Neurosci. *4*, 989–996.

Prybylowski, K., Fu, Z., Losi, G., Hawkins, L.M., Luo, J., Chang, K., Wenthold, R.J., and Vicini, S. (2002). Relationship between availability of NMDA receptor subunits and their expression at the synapse. J. Neurosci. *22*, 8902–8910.

Quinlan, E.M., Olstein, D.H., and Bear, M.F. (1999). Bidirectional, experience-dependent regulation of N-methyl-D-aspartate receptor subunit composition in the rat visual cortex during postnatal development. Proc. Natl. Acad. Sci. USA *96*, 12876–12880.

Rao, A., and Craig, A.M. (1997). Activity regulates the synaptic localization of the NMDA receptor in hippocampal neurons. Neuron *19*, 801–812.

Salter, M.W., and Kalia, L.V. (2004). Src kinases: a hub for NMDA receptor regulation. Nat. Rev. Neurosci. *5*, 317–328.

Sara, Y., Virmani, T., Deák, F., Liu, X., and Kavalali, E.T. (2005). An isolated pool of vesicles recycles at rest and drives spontaneous neurotransmission. Neuron *45*, 563–573.

Schoch, S., Deák, F., Königstorfer, A., Mozhayeva, M., Sara, Y., Südhof, T.C., and Kavalali, E.T. (2001). SNARE function analyzed in synaptobrevin/VAMP knockout mice. Science *294*, 1117–1122.

Sheng, M., Cummings, J., Roldan, L.A., Jan, Y.N., and Jan, L.Y. (1994). Changing subunit composition of heteromeric NMDA receptors during development of rat cortex. Nature *368*, 144–147.

Shepherd, J.D., and Huganir, R.L. (2007). The cell biology of synaptic plasticity: AMPA receptor trafficking. Annu. Rev. Cell Dev. Biol. *23*, 613–643.

Skeberdis, V.A., Chevaleyre, V., Lau, C.G., Goldberg, J.H., Pettit, D.L., Suadicani, S.O., Lin, Y., Bennett, M.V., Yuste, R., Castillo, P.E., and Zukin, R.S. (2006). Protein kinase A regulates calcium permeability of NMDA receptors. Nat. Neurosci. *9*, 501–510.

Sobczyk, A., Scheuss, V., and Svoboda, K. (2005). NMDA receptor subunit-dependent [Ca2+] signaling in individual hippocampal dendritic spines. J. Neurosci. *25*, 6037–6046.

Sutton, M.A., Wall, N.R., Aakalu, G.N., and Schuman, E.M. (2004). Regulation of dendritic protein synthesis by miniature synaptic events. Science *304*, 1979–1983.

Tang, Y.P., Shimizu, E., Dube, G.R., Rampon, C., Kerchner, G.A., Zhuo, M., Liu, G., and Tsien, J.Z. (1999). Genetic enhancement of learning and memory in mice. Nature *401*, 63–69.

Watt, A.J., van Rossum, M.C., MacLeod, K.M., Nelson, S.B., and Turrigiano, G.G. (2000). Activity coregulates quantal AMPA and NMDA currents at neocortical synapses. Neuron *26*, 659–670.

Watt, A.J., Sjöström, P.J., Häusser, M., Nelson, S.B., and Turrigiano, G.G. (2004). A proportional but slower NMDA potentiation follows AMPA potentiation in LTP. Nat. Neurosci. *7*, 518–524.

Wu, Y., Kawakami, R., Shinohara, Y., Fukaya, M., Sakimura, K., Mishina, M., Watanabe, M., Ito, I., and Shigemoto, R. (2005). Target-cell-specific left-right asymmetry of NMDA receptor content in schaffer collateral synapses in epsilon1/NR2A knock-out mice. J. Neurosci. *25*, 9213–9226.

Yashiro, K., and Philpot, B.D. (2008). Regulation of NMDA receptor subunit expression and its implications for LTD, LTP, and metaplasticity. Neuropharmacology *55*, 1081–1094.

Yashiro, K., Corlew, R., and Philpot, B.D. (2005). Visual deprivation modifies both presynaptic glutamate release and the composition of perisynaptic/extrasynaptic NMDA receptors in adult visual cortex. J. Neurosci. *25*, 11684–11692.

Yasuda, R., Nimchinsky, E.A., Scheuss, V., Pologruto, T.A., Oertner, T.G., Sabatini, B.L., and Svoboda, K. (2004). Imaging calcium concentration dynamics in small neuronal compartments. Sci. STKE *2004*, pl5.

Zhou, Y., Takahashi, E., Li, W., Halt, A., Wiltgen, B., Ehninger, D., Li, G.D., Hell, J.W., Kennedy, M.B., and Silva, A.J. (2007). Interactions between the NR2B receptor and CaMKII modulate synaptic plasticity and spatial learning. J. Neurosci. *27*, 13843–13853.

Zucker, R.S. (1999). Calcium- and activity-dependent synaptic plasticity. Curr. Opin. Neurobiol. *9*, 305–313.